



CERN-EP-2016-188
LHCb-PAPER-2016-014
September 8, 2016

Search for Higgs-like bosons decaying into long-lived exotic particles

The LHCb collaboration[†]

Abstract

A search is presented for massive long-lived particles, in the 20–60 GeV/ c^2 mass range with lifetimes between 5 and 100 ps. The dataset used corresponds to 0.62 fb⁻¹ of proton-proton collision data collected by the LHCb detector at $\sqrt{s} = 7$ TeV. The particles are assumed to be pair-produced by the decay of a Higgs-like boson with mass between 80 and 140 GeV/ c^2 . No excess above the background expectation is observed and limits are set on the production cross-section as a function of the long-lived particle mass and lifetime and of the Higgs-like boson mass.

Submitted to Eur. Phys. J. C

© CERN on behalf of the LHCb collaboration, licence CC-BY-4.0.

[†]Authors are listed at the end of this paper.

1 Introduction

The standard model of particle physics (SM) has shown great success in describing physics processes at very short distances. Nevertheless, open questions remain, such as the hierarchy problem, the imprecise unification of gauge couplings, and the absence of candidates for dark matter. Considerable efforts have been made to address these issues, resulting in a large variety of models. Supersymmetry (SUSY), in which the strong and electroweak forces are unified at a renormalisation scale near the Planck scale, provides a possible solution for the hierarchy problem; the minimal supersymmetric standard model (MSSM) is the simplest, phenomenologically viable realisation of SUSY [1, 2].

The present study focuses on a subset of models featuring massive long-lived particles (LLP) with a measurable flight distance. We concentrate on scenarios in which the LLP decays hadronically in the LHCb vertex detector, travelling distances which can be larger than those of typical b hadrons.

A large number of LLP searches have been performed by the experiments at the LHC and Tevatron, mainly using the Hidden Valley framework [3] as a benchmark model [4–8]. Hidden Valley processes have also been sought by LHCb [9], which is able to explore the forward rapidity region only partially covered by other LHC experiments. In addition, it is able to trigger on particles with low transverse momenta, allowing the experiment to probe relatively small LLP masses.

The event topology considered in this study is quite different from that of Hidden Valley models. The minimal supergravity model (mSUGRA) realisation of the MSSM is used as a benchmark model with baryon number violation [10], as suggested in Refs. [11, 12]. Here a Higgs-like boson produced in pp collisions decays into two LLPs (neutralinos), subsequently decaying into three quarks each. The Higgs-like particle mass ranges from $80 \text{ GeV}/c^2$ up to $140 \text{ GeV}/c^2$, covering the mass of the scalar boson discovered by the ATLAS and CMS experiments [13, 14]. The explored LLP lifetime range of 5–100 ps is higher than the typical b hadron lifetime, and corresponds to an average flight distance of up to 30 cm, which is inside the LHCb vertex detector region. The LLP mass range considered is between $20 \text{ GeV}/c^2$ and $60 \text{ GeV}/c^2$.

2 Detector description

The LHCb detector [15, 16] is a single-arm forward spectrometer covering the pseudorapidity range $2 < \eta < 5$, designed for the study of particles containing b or c quarks. The detector includes a high-precision tracking system consisting of a silicon-strip vertex detector surrounding the pp interaction region (VELO), a large-area silicon-strip detector located upstream of a dipole magnet with a bending power of about 4 Tm, and three stations of silicon-strip detectors and straw drift tubes, placed downstream of the magnet. The tracking system provides a measurement of the momentum, p , of charged particles with a relative uncertainty that varies from 0.5% at low momentum to 1.0% at $200 \text{ GeV}/c$. The minimum distance of a track to a primary vertex (PV), the impact parameter, is measured with a resolution of $(15 + 29/p_T) \mu\text{m}$, where p_T is the component of the momentum transverse to the beam, in GeV/c . Different types of charged hadrons are distinguished using information from two ring-imaging Cherenkov detectors. Photons, electrons and hadrons are identified by a calorimeter system consisting of scintillating-pad

and preshower detectors, an electromagnetic calorimeter and a hadronic calorimeter. Muons are identified by a system composed of alternating layers of iron and multiwire proportional chambers. The online event selection is performed by a trigger [17], which consists of a hardware stage, L0, based on information from the calorimeter and muon systems, followed by two software stages, HLT1 and HLT2, which run a simplified version of the offline event reconstruction.

3 Event generation and detector simulation

Various simulated event samples are used in this analysis. The pp collisions are generated with PYTHIA 6 [18]. The process simulated is $h^0 \rightarrow \tilde{\chi}_1^0 \tilde{\chi}_1^0$, where the Higgs-like boson of mass m_{h^0} is produced via gluon-gluon fusion, with the parton density function taken from CTEQ6L [19]. The neutralino $\tilde{\chi}_1^0$ is an LLP of mass m_{LLP} and lifetime τ_{LLP} , which decays into three quarks via the mSUGRA baryon number violating process available in PYTHIA. The corresponding decay flavour structure for the neutralino with a mass of $48 \text{ GeV}/c^2$ is 18.5% for each of the combinations with a b quark (udb , usb , cdb , csb), and 13% for each udq and cdq , where q is not a b quark, *i.e.* about 75% of LLPs have a b quark in the decay. This fraction becomes 70% for $m_{\text{LLP}} = 20 \text{ GeV}/c^2$.

Two separate detector simulations are used, a full simulation where the interaction of the generated particles with the detector is based on GEANT4 [20], and a fast simulation. In GEANT4, the detector and its response are implemented as described in Ref. [21]. Signal models for a representative set of theoretical parameters have been generated and fully simulated (Appendix A, Table 5). In the remainder of this paper, the following nomenclature is chosen: a prefix “BV”, indicating baryon number violation, is followed by the LLP mass in GeV/c^2 and lifetime, and the prefix “mH” followed by the m_{h^0} value in GeV/c^2 . Most of the fully simulated models have $m_{h^0} = 114 \text{ GeV}/c^2$, which is in the middle of the chosen Higgs-like particle mass range. Only events with at least one $\tilde{\chi}_1^0$ in the pseudorapidity region $1.8 < \eta < 5.0$ are processed by GEANT4, corresponding to about 30% of the generated events.

The fast simulation is used to cover a broader parameter space of the theoretical models. Here the charged particles from the $h^0 \rightarrow \tilde{\chi}_1^0 \tilde{\chi}_1^0$ process falling in the geometrical acceptance of the detector are processed by the vertex reconstruction algorithm. The fast simulation is validated by comparison with the full simulation. The detection efficiencies predicted by the full and the fast simulation differ by less than 5% for all the signal models. The distributions for mass, momentum and transverse momentum of the reconstructed LLP, and for the reconstructed vertex position coincide.

Events with direct production of charm, bottom and top quarks are considered as sources of background. Samples of such events were produced and fully simulated. In particular, 17×10^6 inclusive $b\bar{b}$ events (9×10^6 inclusive $c\bar{c}$ events) were produced with at least two b hadrons (c hadrons) in $1.5 < \eta < 5.0$, and half a million $t\bar{t}$ events with at least one muon in the acceptance.

4 Event selection and signal determination

This analysis searches for events with pairs of displaced high-multiplicity vertices. The main background is due to secondary interactions of particles with the detector material.

These events are discarded by a material veto, which rejects vertices in regions occupied by detector material [22]. The remaining candidates are found to be compatible with $b\bar{b}$ events.

From simulation, LLP candidates within the detector acceptance are selected by the L0 and HLT1 triggers with an efficiency of more than 85%. The simulation indicates that the trigger activity is dominated by the hadronic component of the signal expected from high multiplicity events. In HLT2, primary vertices and displaced vertices are reconstructed from charged tracks [23]. Genuine PVs are identified by a small radial distance from the beam axis, $R_{xy} < 0.3$ mm, and must have at least 10 tracks, including at least one forward track (*i.e.* in the direction of the spectrometer) and one backward track. Once the set of PVs is identified, all other reconstructed vertices are candidates for the decay position of LLPs. The preselection requires at least one PV in the event and two LLP candidates. The LLP candidates must have at least four forward tracks, no backward tracks, and a minimum invariant mass reconstructed from charged tracks larger than $3.5 \text{ GeV}/c^2$ for one candidate, and larger than $4.5 \text{ GeV}/c^2$ for the other. In addition, the two secondary vertices must have $R_{xy} > 0.4$ mm and pass the material veto.

The preselection criteria drastically suppress the hadronic background. Only 37 events (74 LLP candidates) survive from the simulated set of 17.1×10^6 $b\bar{b}$ events generated in the LHCb acceptance, corresponding to an integrated luminosity of 0.3 pb^{-1} . Three simulated $c\bar{c}$ events pass the selection. They contain b hadrons and hence belong to the category of inclusive $b\bar{b}$, which is also the case of the two surviving $t\bar{t}$ events. From the 0.62 fb^{-1} data sample, 42.9×10^3 events are selected. The $b\bar{b}$ cross-section value measured by LHCb, $288 \pm 4 \pm 48 \text{ } \mu\text{b}$ [24, 25], predicts $(76 \pm 22) \times 10^3$ events, 1.8 ± 0.5 times the yield observed in data. The estimate uses the next-to-leading-order POWHEG calculation [26] to correct PYTHIA, and the detection efficiency obtained from the simulated events. The measured yield has also been compared to the rate observed in LHCb by a dedicated inclusive $b\bar{b}$ analysis, based on a topological trigger [27]. The consistency with the $b\bar{b}$ background is verified within a statistical precision of 10%.

The shapes of the distributions of the relevant observables are compatible with the $b\bar{b}$ background. Figure 1 compares the distributions for the LLP candidates taken from data and from simulated $b\bar{b}$ events. The distributions for three fully simulated signal models are also shown. The mass and the p_T values are calculated assuming the pion mass for each charged track. Figure 1(d) presents the radial distribution of the displaced vertices; the drop in the number of candidates with a vertex above $R_{xy} \sim 5$ mm is due to the material veto. The variables σ_R and σ_Z shown in Figs. 1(e) and (f) are the position uncertainties provided by the vertex fit in the transverse distance R_{xy} and along the z axis, parallel to the beam. The values of σ_R and σ_Z are larger for the candidates from $b\bar{b}$ background than for the signal because light boosted particles produce close parallel tracks, with the consequence that the vertex fit has larger uncertainties than for the decay of heavier particles producing more diverging tracks. Figure 2 presents the LLP distance of flight and R_{xy} distributions compared to three fully simulated signal models, corresponding to τ_{LLP} values of 5, 10, and 50 ps.

The reconstructed four-vectors of the two LLPs in the event are added to form the Higgs-like candidate (di-LLP), the corresponding invariant mass and p_T distributions are given in Fig. 3.

Further cuts are applied to the preselected data, to increase the statistical sensitivity. The figure of merit used is given by $\epsilon/\sqrt{N_d + 1}$, where ϵ is the signal efficiency from

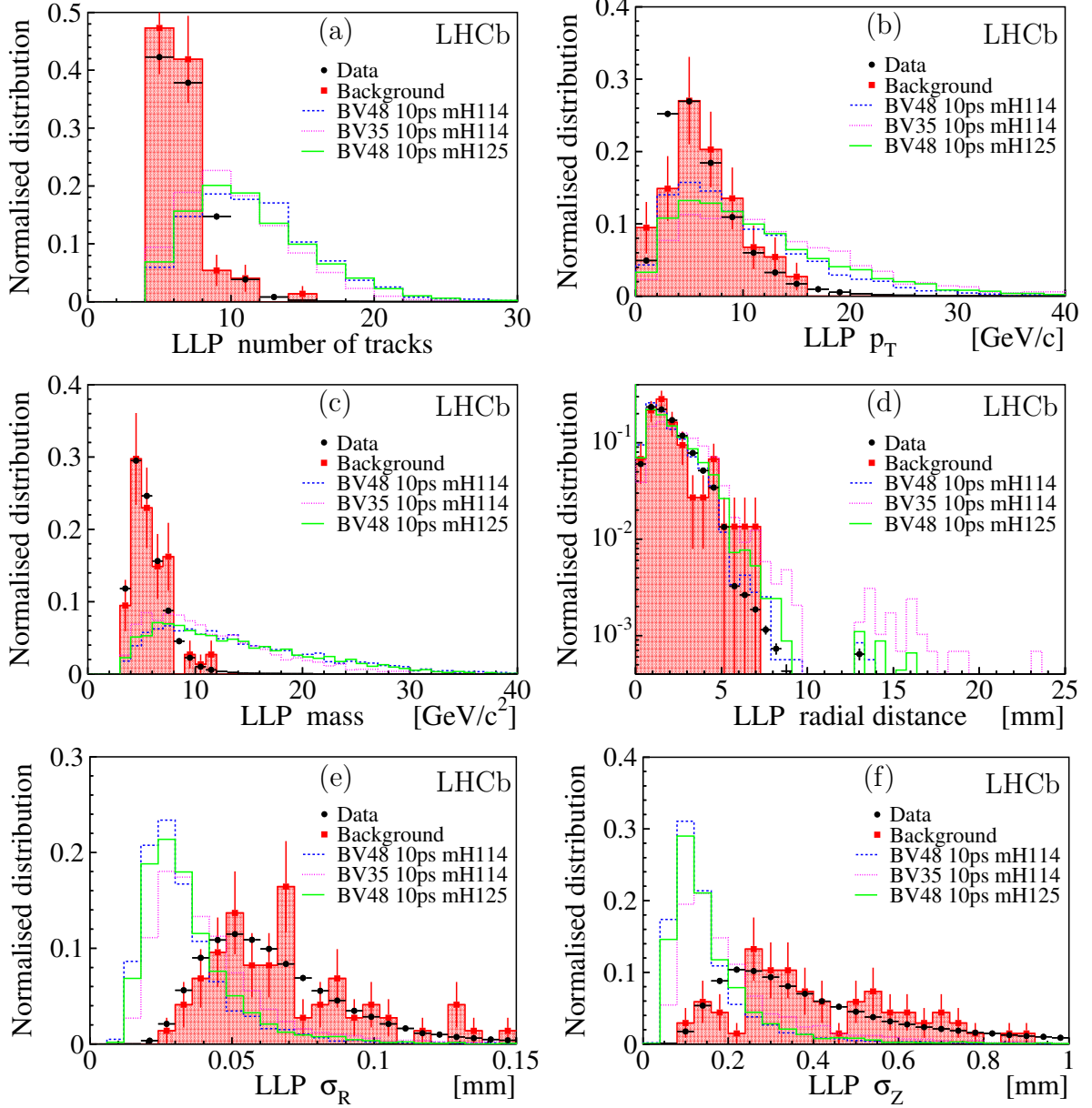


Figure 1: Data (black dots) and simulated distributions after preselection normalised to unit integral. There are two LLP candidates per event. The simulated $b\bar{b}$ background is shown by the filled red histograms with error bars. The dashed (blue), dotted (purple) and solid (green) lines are distributions for fully simulated signal models. The subplots show (a) number of tracks used to reconstruct the LLP candidates, (b) LLP transverse momentum, (c) LLP invariant mass, (d) radial distance, R_{xy} , (e) uncertainty of the radial position, σ_R , and (f) uncertainty of the longitudinal position, σ_Z , of the LLP vertex.

simulation for a given selection, and N_d the corresponding number of candidates found in the data. The baseline selection (Sel₁) is defined by a minimum number of charged tracks on each vertex $N_{\min}^{\text{track}} = 6$, a minimum reconstructed mass $m_{\min}^{\text{LLP}} = 6 \text{ GeV}/c^2$, and maximum uncertainties from the vertex fit $\sigma_{\max}^R = 0.05 \text{ mm}$, and $\sigma_{\max}^Z = 0.25 \text{ mm}$. All the selections used in this analysis are described in Table 1, with the indication of the number

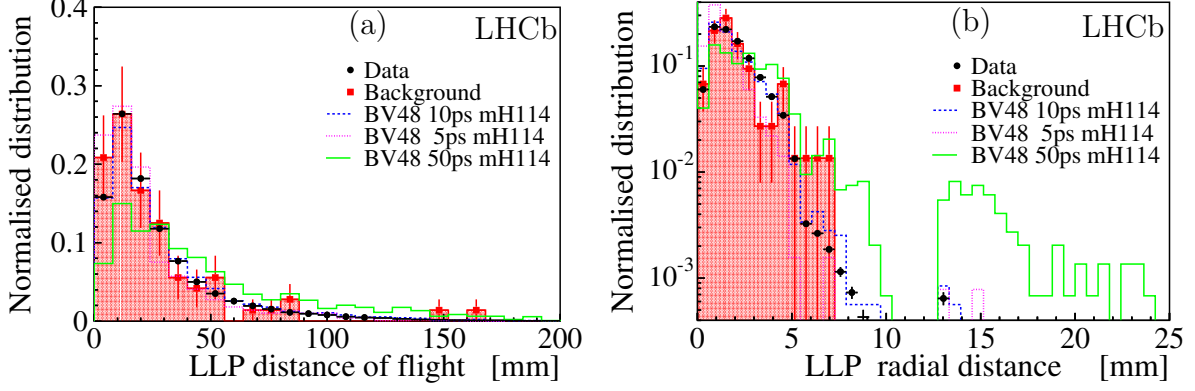


Figure 2: Distributions for (a) the LLP distance of flight from the PV, and, (b), the radial distance of the LLP vertex, R_{xy} . The fully simulated signal models are chosen with LLP lifetimes of 5, 10, and 50 ps. Symbols are defined as in Fig. 1.

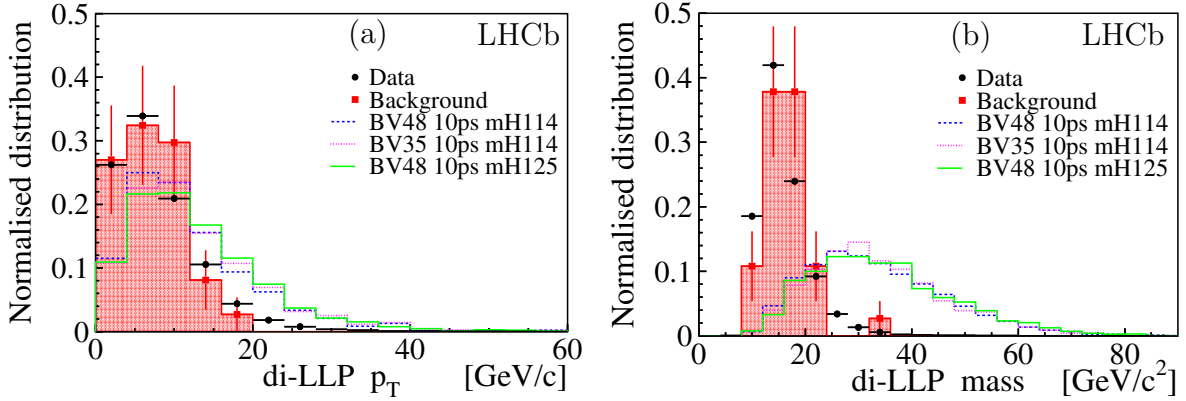


Figure 3: Distributions for (a) the p_T of the Higgs-like candidate, and (b), its invariant mass. Symbols are defined as in Fig. 1.

of data events selected for a di-LLP reconstructed mass above $19 \text{ GeV}/c^2$. Selection Bkg_1 is used to model the background in the fit procedure described in Section 5, selections Sel_2 and Bkg_2 are used to study systematic effects.

5 Determination of the di-LLP signal

The signal yield is determined by a fit of the di-LLP invariant mass, assuming that the two LLPs are the decay products of a narrow resonance. This technique is hampered by the difficulty in producing a reliable background model from simulation, despite the fact that it is reasonable to believe that only $b\bar{b}$ events are the surviving SM component. Therefore, in this analysis the alternative is chosen to infer the background model from data by relaxing the selection requirements, as given by lines Bkg_1 and Bkg_2 of Table 1. The comparison of the results obtained with the different signal and background selections is subsequently used to estimate the systematic effects.

Table 1: Definition of the criteria used for the signal determination. Selections Sel₁ and Bkg₁ are the baseline selections used in the fit, Sel₂ and Bkg₂ are used for the determination of systematic effects. The material veto and the requirement $R_{xy} > 0.4$ mm are applied to both LLP candidates. The last column gives the number of data events selected, for a di-LLP reconstructed mass above 19 GeV/ c^2 .

Selection	N_{\min}^{track}	m_{\min}^{LLP} [GeV/ c^2]	σ_{\max}^{R} [mm]	σ_{\max}^{Z} [mm]	N_{d}
Sel ₁	6	6	0.05	0.25	157
Sel ₂	5	5	0.05	0.25	387
Bkg ₁	4	4	–	–	23.2k
Bkg ₂	5	5	–	–	10.1k

The signal template is the histogram built from BV simulated events selected under the same conditions as data, *i.e.* Sel₁. The background template is the histogram obtained from data events selected by the Bkg₁ conditions. The number of signal (background) candidates N_s (N_b) is determined by an extended maximum likelihood fit. The results are given in Fig. 4 for the BV48 10ps mH114 signal. The fit χ^2/ndf is 0.6. Note that only the portion of the di-LLP mass spectrum above 19 GeV/ c^2 is used, in order to be sufficiently above the mass threshold set by the selections. Alternatively, Sel₂ and Bkg₂ are used to assess systematic effects. The fit results for the selections (Sel₁,Bkg₂), (Sel₂,Bkg₁) are shown in Fig. 5. The corresponding fit χ^2/ndf values are 0.6 and 1.0. The results are given in Table 2 for all fully simulated signal models. All fits give a negative number of signal candidates, compatible with zero. These results are correlated because the data sample is in common and the di-LLP mass shapes are almost identical for the different fully simulated models as depicted in Fig. 3. A check is performed on 142 di-LLP candidates selected from simulated $b\bar{b}$ background without the requirement on R_{xy} and with $m_{\min}^{\text{LLP}} = 4$ GeV/ c^2 for both LLPs. The fitted number of signal events is -0.8 ± 3.5 .

The behaviour and sensitivity of the procedure is further studied by adding a small number of signal events to the data according to a given signal model. Figure 6 shows the results for two models with 10 signal events added to the data. The fitted N_s corresponds well to the number of injected signal events.

An alternative fit procedure has been applied, using parameterised signal and background templates. The sum of two exponential functions is used for the background, and an exponential convolved with a Gaussian function for the signal. The results are consistent with a null signal for all the models.

As a final check a two-dimensional sideband subtraction method (“ABCD method” [28]) has been applied in the reconstructed mass of one LLP and the number of tracks of the other LLP, also giving results consistent with zero signal.

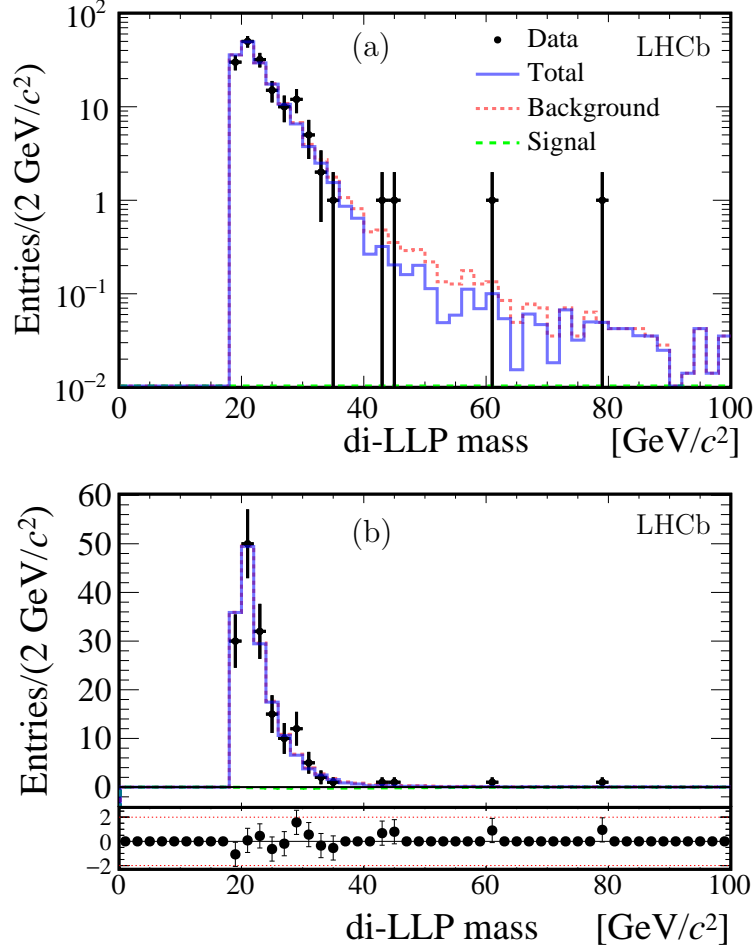


Figure 4: Results of the fit based on the model BV48 10ps mH114. In (a) log distribution and (b) linear scale with pull distribution. Dots with error bars are the data, the dotted (red) and the dashed (green) histograms show the fitted background and signal contributions, respectively. The purple histogram is the total fitted distribution.

6 Detection efficiency and systematic uncertainties

The determination of the detection efficiency is based on simulated events. The geometrical acceptance for the detection of one $\tilde{\chi}_1^0$ in LHCb is, depending on the model, between 20 and 30%. After selection Sel₁ the predicted total di-LLP detection efficiency is in the range 0.1–1% for most of the models. Potential discrepancies between simulation and data are considered as sources of systematic uncertainties. Table 3 summarises the contributions of the systematic uncertainties, which are valid for all fully simulated models, dominated by the 15% contribution from the trigger.

The consistency between the trigger efficiency in data and simulation is checked by selecting LLP events with an independent trigger, designed for the detection of J/ψ events. Comparing the fraction of the data that also passes the double-LLP selection with the corresponding fraction in simulated inclusive J/ψ events, consistent efficiencies are found within a statistical uncertainty of 30%. A more precise result is obtained when requiring only a single LLP candidate [9] and assuming uncorrelated contributions from the two

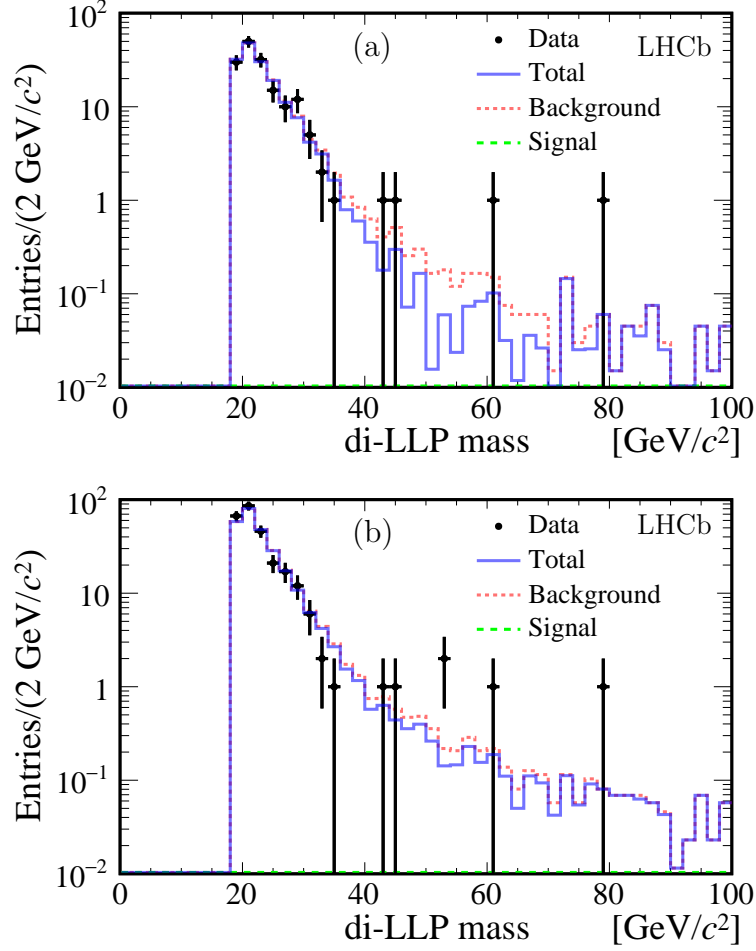


Figure 5: Results of the fit based on the model BV48 10ps mH114, for different combinations of signal and background selections, (a) signal from Sel₁ and background from Bkg₂, (b) signal from Sel₂ and background from Bkg₁. Dots with error bars are data, the dashed (green) line is the fitted signal and the dotted (red) line the background. In both cases the fitted signal is negative. The histogram (blue) is the total fitted function.

LLPs to determine the efficiency for detecting two LLPs in coincidence. A maximum discrepancy between data and simulation of 15% is inferred, which is the value adopted.

The consistency between the track reconstruction efficiency in data and simulation is studied by a comparison of the number of tracks selected in displaced vertices from $b\bar{b}$ events. The average number of tracks per LLP in data is higher than in simulated events by about 0.07 tracks. Assuming that this small effect is entirely due to a difference in tracking efficiency, the overall di-LLP detection efficiency changes by at most 5%.

The vertex reconstruction efficiency is affected by the tracking efficiency and resolution. A study of vertices from $B^0 \rightarrow J/\psi K^{*0}$ with $J/\psi \rightarrow \mu^+\mu^-$ and $K^{*0} \rightarrow K^+\pi^-$ has shown that the data and simulation detection efficiencies for this four-prong process agree within 7.5% [9]. This has been evaluated to correspond at most to a 4% discrepancy between the di-LLP efficiency in data and simulation.

A maximum mismatch of 10% on both the transverse momentum and mass scales is inferred from the comparison of data and simulated $b\bar{b}$ distributions, which propagates to

Table 2: Values of the fitted signal and background events for the different fully simulated signal models. The signal/background combinations are defined in the first row.

Model	(Sel ₁ ,Bkg ₁)		(Sel ₁ ,Bkg ₂)	(Sel ₂ ,Bkg ₁)
	N_s	N_b	N_s	N_s
BV48 5ps mH114	-2.6 ± 4.4	163.6 ± 13.6	-4.8 ± 3.9	-1.7 ± 3.9
BV48 10ps mH114	-3.3 ± 3.5	164.3 ± 13.4	-4.6 ± 3.1	-3.1 ± 3.6
BV48 15ps mH114	-3.5 ± 3.6	164.5 ± 13.5	-4.4 ± 3.1	-2.0 ± 3.6
BV48 50ps mH114	-1.4 ± 3.6	162.4 ± 13.3	-2.7 ± 3.4	-2.1 ± 4.2
BV48 100ps mH114	-0.7 ± 4.1	161.7 ± 13.4	-3.5 ± 3.9	-3.2 ± 4.2
BV35 10ps mH114	-4.3 ± 3.3	165.3 ± 13.4	-5.9 ± 3.1	-4.6 ± 3.5
BV20 10ps mH114	-1.9 ± 1.6	162.8 ± 12.9	-2.7 ± 1.7	-2.0 ± 2.4
BV48 10ps mH100	-1.7 ± 4.7	162.7 ± 13.7	-4.4 ± 4.4	-5.2 ± 4.7
BV48 10ps mH125	-2.8 ± 3.5	163.8 ± 13.4	-4.1 ± 3.2	-3.2 ± 3.6
BV55 10ps mH114	-3.1 ± 3.7	164.1 ± 13.5	-4.6 ± 3.4	-1.1 ± 3.7
BV55 10ps mH125	-2.6 ± 3.5	163.6 ± 13.4	-4.0 ± 3.2	-3.9 ± 3.8

Table 3: Contributions to the systematic uncertainty for fully simulated models. For the analysis based on the fast simulation the same total systematic uncertainty is adopted augmented by 5% to account for the relative imprecision of the fast and full simulations. The contributions from the signal and the data-driven background models used in the di-LLP mass fit are discussed in the text.

Source	(%)
Trigger	15
Track reconstruction	5
Vertex reconstruction	4
p_T and mass calibration	6
Material veto	4
PV multiplicity	0.1
Beam line position	0.7
Theoretical model	9.9
Integrated luminosity	1.7
Total	20.5

a 6% contribution to the systematic uncertainty.

The effect of the material veto corresponds to a reduction of the geometrical acceptance and depends mainly on the LLP lifetime. An analysis with the requirement of $R_{xy} < 4$ mm allows to infer a maximum systematic uncertainty of 4%.

A small contribution to the systematic uncertainty of 0.1% is determined by reweighting the simulated events to match the PV multiplicity in the data.

The uncertainty on the position of the beam line is less than $20 \mu\text{m}$ [29]. It can affect the secondary vertex selection, mainly via the requirement on R_{xy} . By altering the PV

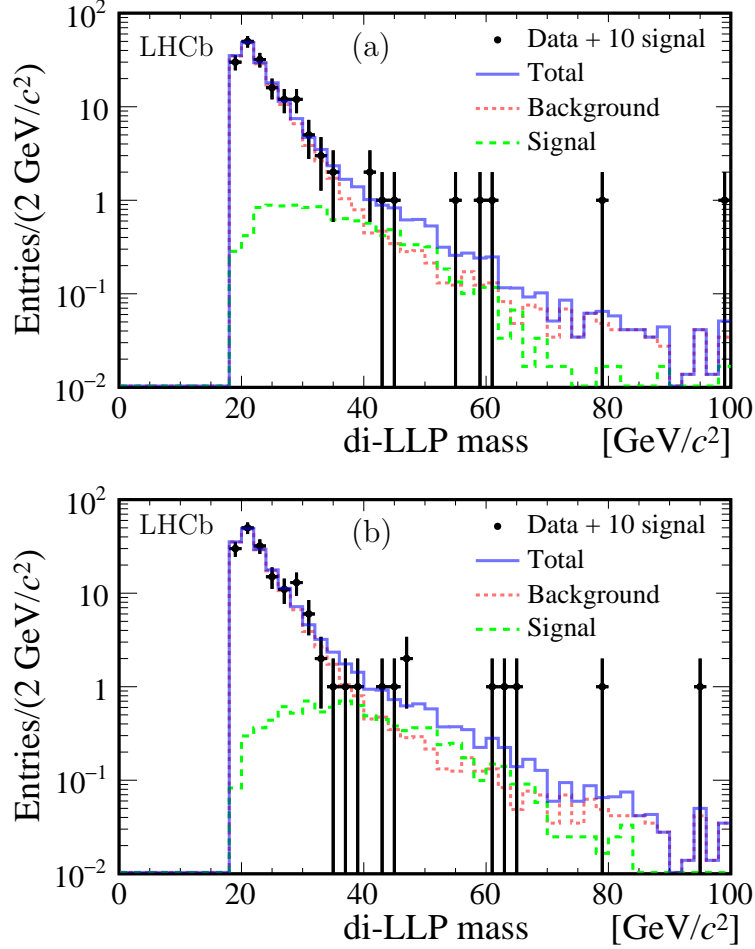


Figure 6: Results of the fit to the data to which 10 signal events have been added randomly chosen following the signal model. For the theoretical model BV48 10ps mH100, in (a), the fitted signal is 11.1 ± 7.0 events; for BV48 10ps mH125, in (b), the result is 9.3 ± 5.6 events.

position in simulated signal events, the maximum effect on the di-LLP selection efficiency is 0.7%.

The Higgs-like particle production model is mainly affected by the uncertainty on the parton luminosity. A maximum variation of the detection efficiency of 9.5% is obtained following the prescriptions given in [30]. A second contribution of 3% is obtained by reweighting the PYTHIA generated events to match a recent calculation of the p_T distributions [31]. The total theoretical uncertainty is 9.9%, obtained by summing in quadrature the mentioned contributions.

In addition to the systematic uncertainty on the detection efficiency, the following contributions have been considered. The uncertainty on the integrated luminosity is 1.7% [32]. As previously stated, the uncertainty on the momentum scale and the invariant mass scale is smaller than 10%. This value is also assumed for the di-LLP mass calibration. To assess the impact on the signal measurement, pseudoexperiments are produced with 10 events of simulated signal added to the background following the nominal signal distribution but with the di-LLP mass value scaled by $\pm 10\%$. The subsequent maximum

variation of the fitted number of events is ± 1.6 , for all the signal hypotheses. The uncertainty due to the shape of the background template is obtained by comparing the number of fitted events obtained with the Bkg₁ and Bkg₂ selections. The change is less than one event, for all the signal models. The difference in data and simulation in the di-LLP mass resolution and the statistical precision of the signal templates used in the fit have a negligible effect. Hence, a fit uncertainty of ± 2 events is considered in the calculation of the cross-section upper limits.

For the analysis based on the fast simulation, a 5% uncertainty is added to account for the relative imprecision of the fast simulation with respect to the full simulation, as explained in Section 3.

7 Results

The 95% confidence level (CL) upper limits on the production cross-section times branching ratio are presented in Table 4, for the fully simulated models, based on the CLs approach [33]. The fast simulation allows the exploration of a larger region of parameter space. The cross-section times branching fraction upper limits at 95% CL for benchmark theoretical models are shown in Fig. 7 (the corresponding tables are given in Appendix C).

The estimated detection efficiencies can be found in Appendix B, Tables 6 and 7. The efficiency increases with m_{LLP} because more particles are produced in the decay of heavier LLPs. This effect is only partially counteracted by the loss of particles outside of the spectrometer acceptance, which is especially the case with heavier Higgs-like particles.

Table 4: Detection efficiency with total uncertainty, and upper limits at 95% CL on the cross-section times branching ratio for the process $pp \rightarrow h^0 X$, $h^0 \rightarrow \tilde{\chi}_1^0 \tilde{\chi}_1^0 \rightarrow 6q$ for the fully simulated models.

Model	Efficiency [%]	Expected upper limit [pb]	Observed upper limit [pb]
BV48 5ps mH114	0.528 ± 0.114	$3.2^{+2.1}_{-1.1}$	3.5
BV48 10ps mH114	0.925 ± 0.194	$1.8^{+1.2}_{-0.6}$	1.7
BV48 15ps mH114	0.966 ± 0.208	$1.8^{+1.2}_{-0.6}$	1.6
BV48 50ps mH114	0.419 ± 0.090	$4.6^{+2.9}_{-1.6}$	4.4
BV48 100ps mH114	0.171 ± 0.037	$11.9^{+7.1}_{-3.8}$	12.3
BV35 10ps mH114	0.268 ± 0.058	$5.6^{+3.8}_{-2.0}$	4.9
BV20 10ps mH114	0.016 ± 0.003	52^{+38}_{-20}	54
BV48 10ps mH100	0.864 ± 0.186	$2.5^{+1.6}_{-0.8}$	2.6
BV48 10ps mH125	0.771 ± 0.166	$2.0^{+1.4}_{-0.7}$	2.0
BV55 10ps mH114	0.851 ± 0.183	$1.9^{+1.3}_{-0.7}$	1.9
BV55 10ps mH125	0.937 ± 0.201	$1.7^{+1.1}_{-0.6}$	1.7

Another competing phenomenon is that the lower boost of heavier LLPs results in a shorter average flight length, *i.e.* the requirement of a minimum R_{xy} disfavours heavy LLPs. The cut on R_{xy} is more efficient at selecting LLPs with large lifetimes, but for lifetimes larger than ~ 50 ps a portion of the decays falls into the material region and is discarded. Finally, a drop of sensitivity is expected for LLPs with a lifetime close to the b hadron lifetimes, where the contamination from $b\bar{b}$ events becomes important, especially for low mass LLPs.

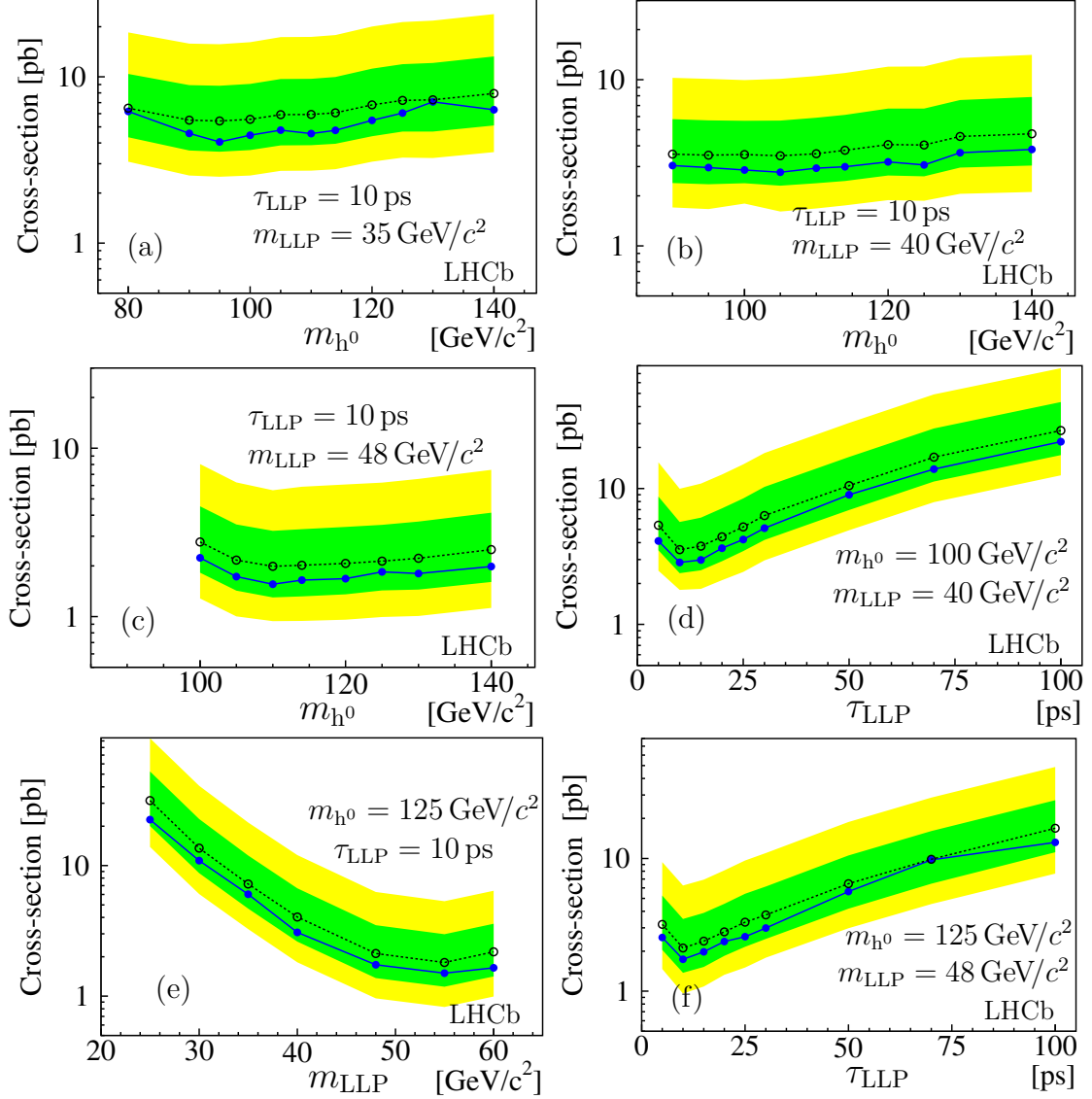


Figure 7: Expected (open dots with 1σ and 2σ bands) and observed (full dots) upper limits at 95% confidence level, (a) – (c) shown for different masses of the Higgs-like particle, (d) and (f) for different LLP lifetimes, and (e) as a function of the LLP mass. The values of the other parameters are indicated on the plots. Results inferred from the fast simulation.

8 Conclusion

A search for Higgs-like bosons decaying into two long-lived particles decaying hadronically has been carried out using data from pp collisions at 7 TeV collected with the LHCb detector, corresponding to a total integrated luminosity of 0.62 fb^{-1} .

The model used to describe the LLP decay is an mSUGRA process in which the lightest neutralino $\tilde{\chi}_1^0$ decays through a baryon number violating coupling to three quarks. Upper limits have been placed on the production cross-section for Higgs-like boson masses from 80 to $140 \text{ GeV}/c^2$, LLP masses in the range $20\text{--}60 \text{ GeV}/c^2$, and LLP lifetimes in the range of $5\text{--}100 \text{ ps}$. The number of candidates is determined by the di-LLP invariant mass fit with signal templates inferred from simulation, and background estimates from data. For the explored parameter space of the theory all results, which are correlated, are consistent with zero. Upper limits at 95% CL for cross-section times branching ratio of 1 to 5 pb are inferred for most of the considered parameter range. They are below 2 pb for the decay of a $125 \text{ GeV}/c^2$ Higgs-like particle in two LLPs with mass in the $48\text{--}60 \text{ GeV}/c^2$ range and 10 ps lifetime.

Acknowledgements

We express our gratitude to our colleagues in the CERN accelerator departments for the excellent performance of the LHC. We thank the technical and administrative staff at the LHCb institutes. We acknowledge support from CERN and from the national agencies: CAPES, CNPq, FAPERJ and FINEP (Brazil); NSFC (China); CNRS/IN2P3 (France); BMBF, DFG and MPG (Germany); INFN (Italy); FOM and NWO (The Netherlands); MNiSW and NCN (Poland); MEN/IFA (Romania); MinES and FANO (Russia); MinECo (Spain); SNSF and SER (Switzerland); NASU (Ukraine); STFC (United Kingdom); NSF (USA). We acknowledge the computing resources that are provided by CERN, IN2P3 (France), KIT and DESY (Germany), INFN (Italy), SURF (The Netherlands), PIC (Spain), GridPP (United Kingdom), RRCKI and Yandex LLC (Russia), CSCS (Switzerland), IFIN-HH (Romania), CBPF (Brazil), PL-GRID (Poland) and OSC (USA). We are indebted to the communities behind the multiple open source software packages on which we depend. Individual groups or members have received support from AvH Foundation (Germany), EPLANET, Marie Skłodowska-Curie Actions and ERC (European Union), Conseil Général de Haute-Savoie, Labex ENIGMASS and OCEVU, Région Auvergne (France), RFBR and Yandex LLC (Russia), GVA, XuntaGal and GENCAT (Spain), Herchel Smith Fund, The Royal Society, Royal Commission for the Exhibition of 1851 and the Leverhulme Trust (United Kingdom).

Appendices

A Fully simulated signal datasets

Table 5 shows the parameters used to generate the 11 fully simulated signal models with PYTHIA 6. The Higgs-like boson is produced by gluon-gluon fusion. In the table M_1 corresponds to the PYTHIA parameter RMSS(1), and $\tan\beta$ to RMSS(5). In addition, M_2 (RMSS(2)) is set at $250 \text{ GeV}/c^2$ and μ (RMSS(4)) has the value 140. A m_{h^0} value of $125 \text{ GeV}/c^2$ requires $\text{RMSS}(16) = 2300$.

Table 5: Parameters of the signal models generated by PYTHIA and fully simulated.

Model	M_1 [GeV/c^2]	$\tan\beta$	m_{h^0} [GeV/c^2]	m_{LLP} [GeV/c^2]	τ_{LLP} [ps]
BV48 5ps mH114	62	5	114	48	5
BV48 10ps mH114	62	5	114	48	10
BV48 15ps mH114	62	5	114	48	15
BV48 50ps mH114	62	5	114	48	50
BV48 100ps mH114	62	5	114	48	100
BV35 10ps mH114	46	5	114	35	10
BV20 10ps mH114	28	5	114	20	10
BV48 10ps mH100	71	2.4	100	48	10
BV48 10ps mH125	60	8	125	48	10
BV55 10ps mH114	71	5.1	114	55	10
BV55 10ps mH125	69	6.2	125	55	10

B Detection efficiencies

Table 6 gives the detection efficiency as a function of m_{h^0} and m_{LLP} , the LLP lifetime is 10 ps. Table 7 gives the efficiency as a function of m_{LLP} and τ_{LLP} , assuming $m_{h^0} = 114 \text{ GeV}/c^2$.

Table 6: Detection efficiency values in percent estimated by the fast simulation as a function of m_{h^0} and m_{LLP} . The LLP lifetime is 10 ps. The statistical uncertainty is 10% for $\epsilon \sim 0.02\%$, 5 % for $\epsilon \sim 0.1\%$, 3% for $\epsilon \sim 0.5\%$, and 2% for $\epsilon \sim 1\%$.

m_{h^0} [GeV/ c^2]	m_{LLP} [GeV/ c^2]							
	20	25	30	35	40	48	55	60
80	0.035	0.126	0.276	0.514	–	–	–	–
90	0.027	0.084	0.213	0.456	0.699	–	–	–
95	0.023	0.077	0.203	0.414	0.689	–	–	–
100	0.025	0.073	0.184	0.368	0.647	0.858	–	–
105	0.018	0.066	0.139	0.324	0.574	1.018	–	–
110	0.017	0.053	0.146	0.291	0.525	1.016	–	–
114	0.014	0.048	0.134	0.259	0.472	0.963	0.817	–
120	0.016	0.047	0.107	0.222	0.402	0.836	1.013	–
125	0.009	0.042	0.097	0.225	0.377	0.765	0.997	–
130	0.014	0.037	0.085	0.191	0.325	0.708	0.914	0.991
140	0.002	0.031	0.075	0.163	0.277	0.566	0.782	0.881

Table 7: Detection efficiency in percent estimated by the fast simulation as a function of the m_{LLP} and τ_{LLP} , for $m_{h^0} = 114 \text{ GeV}/c^2$. The statistical uncertainty is 10% for $\epsilon \sim 0.02\%$, 5 % for $\epsilon \sim 0.1\%$, 3% for $\epsilon \sim 0.5\%$, and 2% for $\epsilon \sim 1\%$.

τ_{LLP} [ps]	m_{LLP} [GeV/ c^2]						
	20	25	30	35	40	48	55
5	0.021	0.053	0.129	0.234	0.366	0.545	0.289
10	0.014	0.048	0.134	0.259	0.472	0.963	0.817
15	0.013	0.042	0.113	0.198	0.389	0.932	1.052
20	0.007	0.035	0.083	0.174	0.338	0.834	1.150
25	0.006	0.034	0.073	0.148	0.289	0.731	1.126
30	0.005	0.026	0.066	0.128	0.241	0.643	1.091
40	0.003	0.017	0.044	0.114	0.193	0.490	0.960
50	0.004	0.015	0.035	0.082	0.157	0.397	0.806
70	0.002	0.009	0.021	0.062	0.104	0.280	0.596
100	0.001	0.005	0.015	0.033	0.071	0.178	0.383

C Cross-section upper limits tables

Expected and observed 95% CL cross-section times branching ratio upper limits for benchmark models, from the fast simulation. Table 8 and 9 give the limits as a function of m_{h^0} , covering LLP masses from 35 to 60 GeV/ c^2 , $\tau_{\text{LLP}} = 10$ ps. Table 10: limits as a function of the LLP lifetime for $m_{h^0} = 100$ GeV/ c^2 and $m_{\text{LLP}} = 40$ GeV/ c^2 , and for $m_{h^0} = 125$ GeV/ c^2 and $m_{\text{LLP}} = 48$ GeV/ c^2 . Table 11: limits as a function of the LLP mass, for $m_{h^0} = 125$ GeV/ c^2 , $\tau_{\text{LLP}} = 10$ ps.

Table 8: Expected and observed 95% CL cross-section times branching ratio upper limits as a function of m_{h^0} , with $m_{\text{LLP}} = 35$ GeV/ c^2 , and $\tau_{\text{LLP}} = 10$ ps, estimated by the fast simulation.

Model	Expected upper limit [pb]	Observed upper limit [pb]
BV35 10ps mH80	$6.49^{+3.94}_{-2.16}$	6.20
BV35 10ps mH90	$5.50^{+3.42}_{-1.89}$	4.56
BV35 10ps mH95	$5.42^{+3.41}_{-1.88}$	4.06
BV35 10ps mH100	$5.55^{+3.52}_{-1.92}$	4.45
BV35 10ps mH105	$5.92^{+3.79}_{-2.06}$	4.78
BV35 10ps mH110	$5.94^{+3.79}_{-2.06}$	4.56
BV35 10ps mH114	$6.07^{+3.92}_{-2.11}$	4.77
BV35 10ps mH120	$6.79^{+4.42}_{-2.39}$	5.47
BV35 10ps mH125	$7.21^{+4.70}_{-2.54}$	6.03
BV35 10ps mH130	$7.28^{+4.83}_{-2.59}$	7.08
BV35 10ps mH140	$7.95^{+5.32}_{-2.85}$	6.35

Table 9: Expected and observed 95% CL cross-section times branching ratio upper limits as a function of m_{h^0} , for LLP masses of 40, 48, 55, and 60 GeV/ c^2 , $\tau_{\text{LLP}} = 10$ ps, estimated by the fast simulation.

Model	Expected upper limit [pb]	Observed upper limit [pb]
BV40 10ps mH90	$3.57^{+2.23}_{-1.18}$	3.04
BV40 10ps mH95	$3.52^{+2.18}_{-1.17}$	2.96
BV40 10ps mH100	$3.55^{+2.12}_{-1.16}$	2.86
BV40 10ps mH105	$3.49^{+2.19}_{-1.18}$	2.77
BV40 10ps mH110	$3.59^{+2.32}_{-1.21}$	2.93
BV40 10ps mH114	$3.76^{+2.38}_{-1.30}$	2.99
BV40 10ps mH120	$4.07^{+2.63}_{-1.42}$	3.20
BV40 10ps mH125	$4.04^{+2.66}_{-1.43}$	3.07
BV40 10ps mH130	$4.55^{+2.98}_{-1.61}$	3.63
BV40 10ps mH140	$4.71^{+3.14}_{-1.69}$	3.79
BV48 10ps mH100	$2.78^{+1.75}_{-0.95}$	2.23
BV48 10ps mH105	$2.17^{+1.36}_{-0.74}$	1.73
BV48 10ps mH110	$1.99^{+1.24}_{-0.69}$	1.56
BV48 10ps mH114	$2.02^{+1.29}_{-0.70}$	1.65
BV48 10ps mH120	$2.07^{+1.34}_{-0.71}$	1.68
BV48 10ps mH125	$2.12^{+1.38}_{-0.74}$	1.74
BV48 10ps mH130	$2.22^{+1.45}_{-0.78}$	1.80
BV48 10ps mH140	$2.49^{+1.65}_{-0.89}$	1.98
BV55 10ps mH130	$1.94^{+1.27}_{-0.69}$	1.76
BV55 10ps mH140	$1.93^{+1.26}_{-0.69}$	1.75
BV60 10ps mH130	$1.79^{+1.16}_{-0.63}$	1.52
BV60 10ps mH140	$1.86^{+1.21}_{-0.66}$	1.48

Table 10: Expected and observed 95% CL cross-section times branching ratio upper limits as a function of the LLP lifetime, for $m_{h^0} = 100 \text{ GeV}/c^2$ and $m_{\text{LLP}} = 40 \text{ GeV}/c^2$, and for $m_{h^0} = 125 \text{ GeV}/c^2$ and $m_{\text{LLP}} = 48 \text{ GeV}/c^2$, estimated by the fast simulation.

Model	Expected upper limit [pb]	Observed upper limit [pb]
BV40 5ps mH100	$5.36^{+3.36}_{-1.85}$	4.11
BV40 10ps mH100	$3.55^{+2.12}_{-1.16}$	2.86
BV40 15ps mH100	$3.76^{+2.34}_{-1.26}$	2.98
BV40 20ps mH100	$4.41^{+2.73}_{-1.49}$	3.63
BV40 25ps mH100	$5.21^{+3.23}_{-1.75}$	4.20
BV40 30ps mH100	$6.32^{+3.95}_{-2.13}$	5.10
BV40 50ps mH100	$10.5^{+6.5}_{-3.6}$	9.0
BV40 70ps mH100	$17.0^{+10.6}_{-5.8}$	13.8
BV40 100ps mH100	$26.7^{+16.5}_{-9.1}$	22.1
BV48 5ps mH125	$3.19^{+2.06}_{-1.14}$	2.54
BV48 10ps mH125	$2.12^{+1.38}_{-0.74}$	1.74
BV48 15ps mH125	$2.38^{+1.50}_{-0.86}$	1.98
BV48 20ps mH125	$2.80^{+1.76}_{-0.95}$	2.37
BV48 25ps mH125	$3.31^{+2.11}_{-1.15}$	2.57
BV48 30ps mH125	$3.76^{+2.38}_{-1.28}$	2.99
BV48 50ps mH125	$6.45^{+4.09}_{-2.26}$	5.63
BV48 70ps mH125	$9.86^{+6.23}_{-3.42}$	9.74
BV48 100ps mH125	$16.9^{+10.6}_{-5.8}$	13.2

Table 11: Expected and observed 95% CL cross-section times branching ratio upper limits as a function of the LLP mass, with $m_{h^0} = 125 \text{ GeV}/c^2$ and $\tau_{\text{LLP}} = 10 \text{ ps}$, estimated by the fast simulation.

Model	Expected upper limit [pb]	Observed upper limit [pb]
BV20 10ps mH125	$95.3^{+64.9}_{-34.7}$	112.6
BV25 10ps mH125	$31.4^{+21.0}_{-11.3}$	22.5
BV30 10ps mH125	$13.6^{+9.1}_{-4.9}$	10.9
BV35 10ps mH125	$7.21^{+4.70}_{-2.54}$	6.03
BV40 10ps mH125	$4.04^{+2.66}_{-1.43}$	3.07
BV48 10ps mH125	$2.12^{+1.38}_{-0.74}$	1.74
BV55 10ps mH125	$1.81^{+1.17}_{-0.63}$	1.50
BV60 10ps mH125	$2.18^{+1.40}_{-0.76}$	1.64

References

- [1] S. Dimopoulos, S. Raby, and F. Wilczek, *Supersymmetry and the scale of unification*, Phys. Rev. D **24** (1981) 1681.
- [2] S. P. Martin, *A Supersymmetry primer*, arXiv:hep-ph/9709356.
- [3] M. J. Strassler and K. M. Zurek, *Discovering the Higgs through highly-displaced vertices*, Phys. Lett. B **661** (2008) 263, arXiv:hep-ph/0605193.
- [4] D0 collaboration, V. M. Abazov *et al.*, *Search for resonant pair production of neutral long-lived particles decaying to $b\bar{b}$ in $p\bar{p}$ collisions at $\sqrt{s}=1.96$ TeV*, Phys. Rev. Lett. **103** (2009) 071801, arXiv:0906.1787.
- [5] CDF collaboration, T. Aaltonen *et al.*, *Search for heavy metastable particles decaying to jet pairs in $p\bar{p}$ collisions at $\sqrt{s}=1.96$ TeV*, Phys. Rev. D **85** (2012) 012007, arXiv:1109.3136.
- [6] CMS collaboration, V. Khachatryan *et al.*, *Search for long-lived neutral particles decaying to quark-antiquark pairs in proton-proton collisions at $\sqrt{s}=8$ TeV*, Phys. Rev. D **91** (2015) 012007, arXiv:1411.6530.
- [7] ATLAS collaboration, G. Aad *et al.*, *Search for pair-produced long-lived neutral particles decaying in the ATLAS hadronic calorimeter in pp collisions at $\sqrt{s}=8$ TeV*, Phys. Lett. B **743** (2015) 15, arXiv:1501.04020.
- [8] ATLAS collaboration, G. Aad *et al.*, *Search for displaced vertices arising from decays of new heavy particles in 7 TeV pp collisions at ATLAS*, Phys. Lett. B **707** (2012) 478, arXiv:1109.2242.
- [9] LHCb collaboration, R. Aaij *et al.*, *Search for long-lived particles decaying to jet pairs*, Eur. Phys. J. C **75** (2014) 152, arXiv:1412.3021.
- [10] L. M. Carpenter, D. E. Kaplan, and E.-J. Rhee, *Six-quark decays of the Higgs boson in Supersymmetry with R -parity violation*, Phys. Rev. Lett. **99** (2007) 211801, arXiv:hep-ph/0607204.
- [11] D. E. Kaplan and K. Rehermann, *Proposal for Higgs and superpartner searches at the LHCb experiment*, JHEP **10** (2007) 056, arXiv:0705.3426.
- [12] P. W. Graham, D. E. Kaplan, S. Rajendran, and P. Saraswat, *Displaced Supersymmetry*, JHEP **07** (2012) 149, arXiv:1204.6038.
- [13] ATLAS collaboration, G. Aad *et al.*, *Observation of a new particle in the search for the Standard Model Higgs boson with the ATLAS detector at the LHC*, Phys. Lett. B **716** (2012) 1, arXiv:1207.7214.
- [14] CMS collaboration, S. Chatrchyan *et al.*, *Observation of a new boson at a mass of 125 GeV with the CMS experiment at the LHC*, Phys. Lett. B **716** (2012) 30, arXiv:1207.7235.

- [15] LHCb collaboration, A. A. Alves Jr. *et al.*, *The LHCb detector at the LHC*, JINST **3** (2008) S08005.
- [16] LHCb collaboration, R. Aaij *et al.*, *LHCb detector performance*, Int. J. Mod. Phys. **A30** (2015) 1530022, [arXiv:1412.6352](#).
- [17] R. Aaij *et al.*, *The LHCb trigger and its performance in 2011*, JINST **8** (2013) P04022, [arXiv:1211.3055](#).
- [18] T. Sjöstrand, S. Mrenna, and P. Skands, *PYTHIA 6.4 physics and manual*, JHEP **05** (2006) 026, [arXiv:hep-ph/0603175](#).
- [19] J. Pumplin *et al.*, *New generation of parton distributions with uncertainties from global QCD analysis*, JHEP **07** (2002) 012, [arXiv:hep-ph/0201195](#).
- [20] Geant4 collaboration, J. Allison *et al.*, *Geant4 developments and applications*, IEEE Trans. Nucl. Sci. **53** (2006) 270; Geant4 collaboration, S. Agostinelli *et al.*, *Geant4: a simulation toolkit*, Nucl. Instrum. Meth. A **506** (2003) 250.
- [21] M. Clemencic *et al.*, *The LHCb simulation application, Gauss: Design, evolution and experience*, J. Phys. Conf. Ser. **331** (2011) 032023.
- [22] LHCb collaboration, R. Aaij *et al.*, *Search for the rare decay $K_S^0 \rightarrow \mu^+ \mu^-$* , JHEP **01** (2013) 090, [arXiv:1209.4029](#).
- [23] M. Kucharczyk, P. Morawski, and M. Witek, *Primary vertex reconstruction at LHCb*, LHCb-PUB-2014-044.
- [24] LHCb collaboration, R. Aaij *et al.*, *Measurement of J/ψ production in pp collisions at $\sqrt{s} = 7$ TeV*, Eur. Phys. J. C **71** (2011) 1645, [arXiv:1103.0423](#).
- [25] LHCb collaboration, R. Aaij *et al.*, *Measurement of $\sigma(pp \rightarrow b\bar{b}X)$ at $\sqrt{s} = 7$ TeV in the forward region*, Phys. Lett. B **694** (2010) 209, [arXiv:1009.2731](#).
- [26] C. Oleari, *The POWHEG BOX*, Nuclear Physics B - Proceedings Supplements **205-206** (2010) 36.
- [27] LHCb collaboration, M. Williams *et al.*, *The HLT2 topological lines*, LHCb-PUB-2011-002.
- [28] ATLAS collaboration, G. Aad *et al.*, *Measurement of the inclusive isolated prompt photon cross section in pp collisions at $\sqrt{s} = 7$ TeV with the ATLAS detector*, Phys. Rev. D **83** (2011) 052005, [arXiv:1012.4389](#).
- [29] R. Aaij *et al.*, *Performance of the LHCb Vertex Locator*, JINST **9** (2014) P09007, [arXiv:1405.7808](#).
- [30] M. Botje *et al.*, *The PDF4LHC working group interim recommendations*, [arXiv:1101.0538](#).
- [31] D. Neill, I. Z. Rothstein, and V. Vaidya, *The Higgs transverse momentum distribution at NNLL and its theoretical errors*, JHEP **12** (2015) 097, [arXiv:1503.00005](#).

- [32] LHCb collaboration, R. Aaij *et al.*, *Precision luminosity measurements at LHCb*, JINST **9** (2014) P12005, [arXiv:1410.0149](#).
- [33] A. L. Read, *Presentation of search results: The CL_s technique*, J. Phys. G **28** (2002) 2693.

LHCb collaboration

R. Aaij³⁹, B. Adeva³⁸, M. Adinolfi⁴⁷, Z. Ajaltouni⁵, S. Akar⁶, J. Albrecht¹⁰, F. Alessio³⁹, M. Alexander⁵², S. Ali⁴², G. Alkhazov³¹, P. Alvarez Cartelle⁵⁴, A.A. Alves Jr⁵⁸, S. Amato², S. Amerio²³, Y. Amhis⁷, L. An⁴⁰, L. Anderlini¹⁸, G. Andreassi⁴⁰, M. Andreotti^{17,g}, J.E. Andrews⁵⁹, R.B. Appleby⁵⁵, O. Aquines Gutierrez¹¹, F. Archilli¹, P. d'Argent¹², J. Arnau Romeu⁶, A. Artamonov³⁶, M. Artuso⁶⁰, E. Aslanides⁶, G. Auriemma^{26,s}, M. Baalouch⁵, S. Bachmann¹², J.J. Back⁴⁹, A. Badalov³⁷, C. Baesso⁶¹, W. Baldini¹⁷, R.J. Barlow⁵⁵, C. Barschel³⁹, S. Barsuk⁷, W. Barter³⁹, V. Batozskaya²⁹, V. Battista⁴⁰, A. Bay⁴⁰, L. Beaucourt⁴, J. Beddow⁵², F. Bedeschi²⁴, I. Bediaga¹, L.J. Bel⁴², V. Belle⁴⁰, N. Belloli^{21,i}, K. Belous³⁶, I. Belyaev³², E. Ben-Haim⁸, G. Bencivenni¹⁹, S. Benson³⁹, J. Benton⁴⁷, A. Berezhnoy³³, R. Bernet⁴¹, A. Bertolin²³, M.-O. Bettler³⁹, M. van Beuzekom⁴², I. Bezshyiko⁴¹, S. Bifani⁴⁶, P. Billoir⁸, T. Bird⁵⁵, A. Birnkraut¹⁰, A. Bitadze⁵⁵, A. Bizzeti^{18,u}, T. Blake⁴⁹, F. Blanc⁴⁰, J. Blouw¹¹, S. Blusk⁶⁰, V. Bocci²⁶, T. Boettcher⁵⁷, A. Bondar³⁵, N. Bondar^{31,39}, W. Bonivento¹⁶, S. Borghi⁵⁵, M. Borisyak⁶⁷, M. Borsato³⁸, F. Bossu⁷, M. Boubdir⁹, T.J.V. Bowcock⁵³, E. Bowen⁴¹, C. Bozzi^{17,39}, S. Braun¹², M. Britsch¹², T. Britton⁶⁰, J. Brodzicka⁵⁵, E. Buchanan⁴⁷, C. Burr⁵⁵, A. Bursche², J. Buytaert³⁹, S. Cadeddu¹⁶, R. Calabrese^{17,g}, M. Calvi^{21,i}, M. Calvo Gomez^{37,m}, P. Campana¹⁹, D. Campora Perez³⁹, L. Capriotti⁵⁵, A. Carbone^{15,e}, G. Carboni^{25,j}, R. Cardinale^{20,h}, A. Cardini¹⁶, P. Carniti^{21,i}, L. Carson⁵¹, K. Carvalho Akiba², G. Casse⁵³, L. Cassina^{21,i}, L. Castillo Garcia⁴⁰, M. Cattaneo³⁹, Ch. Cauet¹⁰, G. Cavallero²⁰, R. Cenci^{24,t}, M. Charles⁸, Ph. Charpentier³⁹, G. Chatzikonstantinidis⁴⁶, M. Chefdeville⁴, S. Chen⁵⁵, S.-F. Cheung⁵⁶, V. Chobanova³⁸, M. Chrzasczcz^{41,27}, X. Cid Vidal³⁸, G. Ciezarek⁴², P.E.L. Clarke⁵¹, M. Clemencic³⁹, H.V. Cliff⁴⁸, J. Closier³⁹, V. Coco⁵⁸, J. Cogan⁶, E. Cogneras⁵, V. Cogoni^{16,f}, L. Cojocariu³⁰, G. Collazuol^{23,o}, P. Collins³⁹, A. Comerma-Montells¹², A. Contu³⁹, A. Cook⁴⁷, S. Coquereau⁸, G. Corti³⁹, M. Corvo^{17,g}, C.M. Costa Sobral⁴⁹, B. Couturier³⁹, G.A. Cowan⁵¹, D.C. Craik⁵¹, A. Crocombe⁴⁹, M. Cruz Torres⁶¹, S. Cunliffe⁵⁴, R. Currie⁵⁴, C. D'Ambrosio³⁹, E. Dall'Occo⁴², J. Dalseno⁴⁷, P.N.Y. David⁴², A. Davis⁵⁸, O. De Aguiar Francisco², K. De Bruyn⁶, S. De Capua⁵⁵, M. De Cian¹², J.M. De Miranda¹, L. De Paula², P. De Simone¹⁹, C.-T. Dean⁵², D. Decamp⁴, M. Deckenhoff¹⁰, L. Del Buono⁸, M. Demmer¹⁰, D. Derkach⁶⁷, O. Deschamps⁵, F. Dettori³⁹, B. Dey²², A. Di Canto³⁹, H. Dijkstra³⁹, F. Dordei³⁹, M. Dorigo⁴⁰, A. Dosil Suárez³⁸, A. Dovbnya⁴⁴, K. Dreimanis⁵³, L. Dufour⁴², G. Dujany⁵⁵, K. Dungs³⁹, P. Durante³⁹, R. Dzhelezhyan³⁶, A. Dziurda³⁹, A. Dzyuba³¹, N. Deléage⁴, S. Easo⁵⁰, U. Egede⁵⁴, V. Egorychev³², S. Eidelman³⁵, S. Eisenhardt⁵¹, U. Eitschberger¹⁰, R. Ekelhof¹⁰, L. Eklund⁵², Ch. Elsasser⁴¹, S. Ely⁶⁰, S. Esen¹², H.M. Evans⁴⁸, T. Evans⁵⁶, A. Falabella¹⁵, N. Farley⁴⁶, S. Farry⁵³, R. Fay⁵³, D. Ferguson⁵¹, V. Fernandez Albor³⁸, F. Ferrari^{15,39}, F. Ferreira Rodrigues¹, M. Ferro-Luzzi³⁹, S. Filippov³⁴, M. Fiore^{17,g}, M. Fiorini^{17,g}, M. Firlej²⁸, C. Fitzpatrick⁴⁰, T. Fiutowski²⁸, F. Fleuret^{7,b}, K. Fohl³⁹, M. Fontana¹⁶, F. Fontanelli^{20,h}, D.C. Forshaw⁶⁰, R. Forty³⁹, M. Frank³⁹, C. Frei³⁹, M. Frosini¹⁸, J. Fu^{22,q}, E. Furfaro^{25,j}, C. Färber³⁹, A. Gallas Torreira³⁸, D. Galli^{15,e}, S. Gallorini²³, S. Gambetta⁵¹, M. Gandelman², P. Gandini⁵⁶, Y. Gao³, J. García Pardiñas³⁸, J. Garra Tico⁴⁸, L. Garrido³⁷, P.J. Garsed⁴⁸, D. Gascon³⁷, C. Gaspar³⁹, L. Gavardi¹⁰, G. Gazzoni⁵, D. Gerick¹², E. Gersabeck¹², M. Gersabeck⁵⁵, T. Gershon⁴⁹, Ph. Ghez⁴, S. Gianì⁴⁰, V. Gibson⁴⁸, O.G. Girard⁴⁰, L. Giubega³⁰, K. Gizdov⁵¹, V.V. Gligorov⁸, D. Golubkov³², A. Golutvin^{54,39}, A. Gomes^{1,a}, I.V. Gorelov³³, C. Gotti^{21,i}, M. Grabalosa Gándara⁵, R. Graciani Diaz³⁷, L.A. Granado Cardoso³⁹, E. Graugés³⁷, E. Graverini⁴¹, G. Graziani¹⁸, A. Grecu³⁰, P. Griffith⁴⁶, L. Grillo¹², B.R. Gruberg Cazon⁵⁶, O. Grünberg⁶⁵, E. Gushchin³⁴, Yu. Guz³⁶, T. Gys³⁹, C. Göbel⁶¹, T. Hadavizadeh⁵⁶, C. Hadjivasiliou⁶⁰, G. Haefeli⁴⁰, C. Haen³⁹, S.C. Haines⁴⁸, S. Hall⁵⁴, B. Hamilton⁵⁹, X. Han¹², S. Hansmann-Menzemer¹², N. Harnew⁵⁶, S.T. Harnew⁴⁷, J. Harrison⁵⁵, J. He⁶², T. Head⁴⁰, A. Heister⁹, K. Hennessy⁵³, P. Henrard⁵, L. Henry⁸,

J.A. Hernando Morata³⁸, E. van Herwijnen³⁹, M. Heß⁶⁵, A. Hicheur², D. Hill⁵⁶, C. Hombach⁵⁵,
 W. Hulsbergen⁴², T. Humair⁵⁴, M. Hushchyn⁶⁷, N. Hussain⁵⁶, D. Hutchcroft⁵³, M. Idzik²⁸,
 P. Ilten⁵⁷, R. Jacobsson³⁹, A. Jaeger¹², J. Jalocha⁵⁶, E. Jans⁴², A. Jawahery⁵⁹, M. John⁵⁶,
 D. Johnson³⁹, C.R. Jones⁴⁸, C. Joram³⁹, B. Jost³⁹, N. Jurik⁶⁰, S. Kandybei⁴⁴, W. Kanso⁶,
 M. Karacson³⁹, J.M. Kariuki⁴⁷, S. Karodia⁵², M. Kecke¹², M. Kelsey⁶⁰, I.R. Kenyon⁴⁶,
 M. Kenzie³⁹, T. Ketel⁴³, E. Khairullin⁶⁷, B. Khanji^{21,39,i}, C. Khurewathanakul⁴⁰, T. Kirn⁹,
 S. Klaver⁵⁵, K. Klimaszewski²⁹, S. Koliiev⁴⁵, M. Kolpin¹², I. Komarov⁴⁰, R.F. Koopman⁴³,
 P. Koppenburg⁴², A. Kozachuk³³, M. Kozeiha⁵, L. Kravchuk³⁴, K. Kreplin¹², M. Kreps⁴⁹,
 P. Krokovny³⁵, F. Kruse¹⁰, W. Krzemien²⁹, W. Kucewicz^{27,l}, M. Kucharczyk²⁷,
 V. Kudryavtsev³⁵, A.K. Kuonen⁴⁰, K. Kurek²⁹, T. Kvaratskheliya^{32,39}, D. Lacarrere³⁹,
 G. Lafferty^{55,39}, A. Lai¹⁶, D. Lambert⁵¹, G. Lanfranchi¹⁹, C. Langenbruch⁴⁹, B. Langhans³⁹,
 T. Latham⁴⁹, C. Lazzeroni⁴⁶, R. Le Gac⁶, J. van Leerdam⁴², J.-P. Lees⁴, A. Leflat^{33,39},
 J. Lefrançois⁷, R. Lefèvre⁵, F. Lemaitre³⁹, E. Lemos Cid³⁸, O. Leroy⁶, T. Lesiak²⁷,
 B. Leverington¹², Y. Li⁷, T. Likhomanenko^{67,66}, R. Lindner³⁹, C. Linn³⁹, F. Lionetto⁴¹,
 B. Liu¹⁶, X. Liu³, D. Loh⁴⁹, I. Longstaff⁵², J.H. Lopes², D. Lucchesi^{23,o}, M. Lucio Martinez³⁸,
 H. Luo⁵¹, A. Lupato²³, E. Luppi^{17,g}, O. Lupton⁵⁶, A. Lusiani²⁴, X. Lyu⁶², F. Machefert⁷,
 F. Maciuc³⁰, O. Maev³¹, K. Maguire⁵⁵, S. Malde⁵⁶, A. Malinin⁶⁶, T. Maltsev³⁵, G. Manca⁷,
 G. Mancinelli⁶, P. Manning⁶⁰, J. Maratas⁵, J.F. Marchand⁴, U. Marconi¹⁵, C. Marin Benito³⁷,
 P. Marino^{24,t}, J. Marks¹², G. Martellotti²⁶, M. Martin⁶, M. Martinelli⁴⁰, D. Martinez Santos³⁸,
 F. Martinez Vidal⁶⁸, D. Martins Tostes², L.M. Massacrier⁷, A. Massafferri¹, R. Matev³⁹,
 A. Mathad⁴⁹, Z. Mathe³⁹, C. Matteuzzi²¹, A. Mauri⁴¹, B. Maurin⁴⁰, A. Mazurov⁴⁶,
 M. McCann⁵⁴, J. McCarthy⁴⁶, A. McNab⁵⁵, R. McNulty¹³, B. Meadows⁵⁸, F. Meier¹⁰,
 M. Meissner¹², D. Melnychuk²⁹, M. Merk⁴², E. Michielin²³, D.A. Milanes⁶⁴, M.-N. Minard⁴,
 D.S. Mitzel¹², J. Molina Rodriguez⁶¹, I.A. Monroy⁶⁴, S. Monteil⁵, M. Morandin²³,
 P. Morawski²⁸, A. Mordà⁶, M.J. Morello^{24,t}, J. Moron²⁸, A.B. Morris⁵¹, R. Mountain⁶⁰,
 F. Muheim⁵¹, M. Mulder⁴², M. Mussini¹⁵, D. Müller⁵⁵, J. Müller¹⁰, K. Müller⁴¹, V. Müller¹⁰,
 P. Naik⁴⁷, T. Nakada⁴⁰, R. Nandakumar⁵⁰, A. Nandi⁵⁶, I. Nasteva², M. Needham⁵¹, N. Neri²²,
 S. Neubert¹², N. Neufeld³⁹, M. Neuner¹², A.D. Nguyen⁴⁰, C. Nguyen-Mau^{40,n}, V. Niess⁵,
 S. Nieswand⁹, R. Niet¹⁰, N. Nikitin³³, T. Nikodem¹², A. Novoselov³⁶, D.P. O’Hanlon⁴⁹,
 A. Oblakowska-Mucha²⁸, V. Obraztsov³⁶, S. Ogilvy¹⁹, R. Oldeman⁴⁸, C.J.G. Onderwater⁶⁹,
 J.M. Otalora Goicochea², A. Otto³⁹, P. Owen⁴¹, A. Oyanguren⁶⁸, A. Palano^{14,d}, F. Palombo^{22,q},
 M. Palutan¹⁹, J. Panman³⁹, A. Papanestis⁵⁰, M. Pappagallo⁵², L.L. Pappalardo^{17,g},
 C. Pappenheimer⁵⁸, W. Parker⁵⁹, C. Parkes⁵⁵, G. Passaleva¹⁸, G.D. Patel⁵³, M. Patel⁵⁴,
 C. Patrignani^{15,e}, A. Pearce^{55,50}, A. Pellegrino⁴², G. Penso^{26,k}, M. Pepe Altarelli³⁹,
 S. Perazzini³⁹, P. Perret⁵, L. Pescatore⁴⁶, K. Petridis⁴⁷, A. Petrolini^{20,h}, A. Petrov⁶⁶,
 M. Petruzzio^{22,q}, E. Picatoste Olloqui³⁷, B. Pietrzyk⁴, M. Pikies²⁷, D. Pinci²⁶, A. Pistone²⁰,
 A. Piucci¹², S. Playfer⁵¹, M. Plo Casasus³⁸, T. Poikela³⁹, F. Polci⁸, A. Poluektov^{49,35},
 I. Polyakov³², E. Polycarpo², G.J. Pomery⁴⁷, A. Popov³⁶, D. Popov^{11,39}, B. Popovici³⁰,
 C. Potterat², E. Price⁴⁷, J.D. Price⁵³, J. Prisciandaro³⁸, A. Pritchard⁵³, C. Prouve⁴⁷,
 V. Pugatch⁴⁵, A. Puig Navarro⁴⁰, G. Punzi^{24,p}, W. Qian⁵⁶, R. Quagliani^{7,47}, B. Rachwal²⁷,
 J.H. Rademacker⁴⁷, M. Rama²⁴, M. Ramos Pernas³⁸, M.S. Rangel², I. Raniuk⁴⁴, G. Raven⁴³,
 F. Redi⁵⁴, S. Reichert¹⁰, A.C. dos Reis¹, C. Remon Alepuz⁶⁸, V. Renaudin⁷, S. Ricciardi⁵⁰,
 S. Richards⁴⁷, M. Rihl³⁹, K. Rinnert^{53,39}, V. Rives Molina³⁷, P. Robbe^{7,39}, A.B. Rodrigues¹,
 E. Rodrigues⁵⁸, J.A. Rodriguez Lopez⁶⁴, P. Rodriguez Perez⁵⁵, A. Rogozhnikov⁶⁷, S. Roiser³⁹,
 V. Romanovskiy³⁶, A. Romero Vidal³⁸, J.W. Ronayne¹³, M. Rotondo²³, T. Ruf³⁹,
 P. Ruiz Valls⁶⁸, J.J. Saborido Silva³⁸, N. Sagidova³¹, B. Saitta^{16,f}, V. Salustino Guimaraes²,
 C. Sanchez Mayordomo⁶⁸, B. Sanmartin Sedes³⁸, R. Santacesaria²⁶, C. Santamarina Rios³⁸,
 M. Santimaria¹⁹, E. Santovetti^{25,j}, A. Sarti^{19,k}, C. Satriano^{26,s}, A. Satta²⁵, D.M. Saunders⁴⁷,
 D. Savrina^{32,33}, S. Schael⁹, M. Schiller³⁹, H. Schindler³⁹, M. Schlupp¹⁰, M. Schmelling¹¹,
 T. Schmelzer¹⁰, B. Schmidt³⁹, O. Schneider⁴⁰, A. Schopper³⁹, M. Schubiger⁴⁰, M.-H. Schune⁷,

R. Schwemmer³⁹, B. Sciascia¹⁹, A. Sciubba^{26,k}, A. Semennikov³², A. Sergi⁴⁶, N. Serra⁴¹, J. Serrano⁶, L. Sestini²³, P. Seyfert²¹, M. Shapkin³⁶, I. Shapoval^{17,44,g}, Y. Shcheglov³¹, T. Shears⁵³, L. Shekhtman³⁵, V. Shevchenko⁶⁶, A. Shires¹⁰, B.G. Siddi¹⁷, R. Silva Coutinho⁴¹, L. Silva de Oliveira², G. Simi^{23,o}, M. Sirendi⁴⁸, N. Skidmore⁴⁷, T. Skwarnicki⁶⁰, E. Smith⁵⁴, I.T. Smith⁵¹, J. Smith⁴⁸, M. Smith⁵⁵, H. Snoek⁴², M.D. Sokoloff⁵⁸, F.J.P. Soler⁵², D. Souza⁴⁷, B. Souza De Paula², B. Spaan¹⁰, P. Spradlin⁵², S. Sridharan³⁹, F. Stagni³⁹, M. Stahl¹², S. Stahl³⁹, P. Stefko⁴⁰, S. Stefkova⁵⁴, O. Steinkamp⁴¹, O. Stenyakin³⁶, S. Stevenson⁵⁶, S. Stoica³⁰, S. Stone⁶⁰, B. Storaci⁴¹, S. Stracka^{24,t}, M. Straticiuc³⁰, U. Straumann⁴¹, L. Sun⁵⁸, W. Sutcliffe⁵⁴, K. Swientek²⁸, V. Syropoulos⁴³, M. Szczekowski²⁹, T. Szumlak²⁸, S. T'Jampens⁴, A. Tayduganov⁶, T. Tekampe¹⁰, G. Tellarini^{17,g}, F. Teubert³⁹, C. Thomas⁵⁶, E. Thomas³⁹, J. van Tilburg⁴², V. Tisserand⁴, M. Tobin⁴⁰, S. Tolk⁴⁸, L. Tomassetti^{17,g}, D. Tonelli³⁹, S. Topp-Joergensen⁵⁶, E. Tournefier⁴, S. Tourneur⁴⁰, K. Trabelsi⁴⁰, M. Traill⁵², M.T. Tran⁴⁰, M. Tresch⁴¹, A. Trisovic³⁹, A. Tsaregorodtsev⁶, P. Tsopelas⁴², A. Tully⁴⁸, N. Tuning⁴², A. Ukleja²⁹, A. Ustyuzhanin^{67,66}, U. Uwer¹², C. Vacca^{16,39,f}, V. Vagnoni^{15,39}, S. Valat³⁹, G. Valenti¹⁵, A. Vallier⁷, R. Vazquez Gomez¹⁹, P. Vazquez Regueiro³⁸, S. Vecchi¹⁷, M. van Veghel⁴², J.J. Velthuis⁴⁷, M. Veltri^{18,r}, G. Veneziano⁴⁰, A. Venkateswaran⁶⁰, M. Vesterinen¹², B. Viaud⁷, D. Vieira¹, M. Vieites Diaz³⁸, X. Vilasis-Cardona^{37,m}, V. Volkov³³, A. Vollhardt⁴¹, B. Voneki³⁹, D. Voong⁴⁷, A. Vorobyev³¹, V. Vorobyev³⁵, C. Voß⁶⁵, J.A. de Vries⁴², C. Vázquez Sierra³⁸, R. Waldi⁶⁵, C. Wallace⁴⁹, R. Wallace¹³, J. Walsh²⁴, J. Wang⁶⁰, D.R. Ward⁴⁸, H.M. Wark⁵³, N.K. Watson⁴⁶, D. Websdale⁵⁴, A. Weiden⁴¹, M. Whitehead³⁹, J. Wicht⁴⁹, G. Wilkinson^{56,39}, M. Wilkinson⁶⁰, M. Williams³⁹, M.P. Williams⁴⁶, M. Williams⁵⁷, T. Williams⁴⁶, F.F. Wilson⁵⁰, J. Kimberley⁵⁹, J. Wishahi¹⁰, W. Wislicki²⁹, M. Witek²⁷, G. Wormser⁷, S.A. Wotton⁴⁸, K. Wraight⁵², S. Wright⁴⁸, K. Wyllie³⁹, Y. Xie⁶³, Z. Xing⁶⁰, Z. Xu⁴⁰, Z. Yang³, H. Yin⁶³, J. Yu⁶³, X. Yuan³⁵, O. Yushchenko³⁶, M. Zangoli¹⁵, K.A. Zarebski⁴⁶, M. Zavertyaev^{11,c}, L. Zhang³, Y. Zhang⁷, Y. Zhang⁶², A. Zhelezov¹², Y. Zheng⁶², A. Zhokhov³², V. Zhukov⁹, S. Zucchelli¹⁵.

¹ Centro Brasileiro de Pesquisas Físicas (CBPF), Rio de Janeiro, Brazil

² Universidade Federal do Rio de Janeiro (UFRJ), Rio de Janeiro, Brazil

³ Center for High Energy Physics, Tsinghua University, Beijing, China

⁴ LAPP, Université Savoie Mont-Blanc, CNRS/IN2P3, Annecy-Le-Vieux, France

⁵ Clermont Université, Université Blaise Pascal, CNRS/IN2P3, LPC, Clermont-Ferrand, France

⁶ CPPM, Aix-Marseille Université, CNRS/IN2P3, Marseille, France

⁷ LAL, Université Paris-Sud, CNRS/IN2P3, Orsay, France

⁸ LPNHE, Université Pierre et Marie Curie, Université Paris Diderot, CNRS/IN2P3, Paris, France

⁹ I. Physikalisches Institut, RWTH Aachen University, Aachen, Germany

¹⁰ Fakultät Physik, Technische Universität Dortmund, Dortmund, Germany

¹¹ Max-Planck-Institut für Kernphysik (MPIK), Heidelberg, Germany

¹² Physikalisches Institut, Ruprecht-Karls-Universität Heidelberg, Heidelberg, Germany

¹³ School of Physics, University College Dublin, Dublin, Ireland

¹⁴ Sezione INFN di Bari, Bari, Italy

¹⁵ Sezione INFN di Bologna, Bologna, Italy

¹⁶ Sezione INFN di Cagliari, Cagliari, Italy

¹⁷ Sezione INFN di Ferrara, Ferrara, Italy

¹⁸ Sezione INFN di Firenze, Firenze, Italy

¹⁹ Laboratori Nazionali dell'INFN di Frascati, Frascati, Italy

²⁰ Sezione INFN di Genova, Genova, Italy

²¹ Sezione INFN di Milano Bicocca, Milano, Italy

²² Sezione INFN di Milano, Milano, Italy

²³ Sezione INFN di Padova, Padova, Italy

²⁴ Sezione INFN di Pisa, Pisa, Italy

²⁵ Sezione INFN di Roma Tor Vergata, Roma, Italy

²⁶ Sezione INFN di Roma La Sapienza, Roma, Italy

- ²⁷ Henryk Niewodniczanski Institute of Nuclear Physics Polish Academy of Sciences, Kraków, Poland
- ²⁸ AGH - University of Science and Technology, Faculty of Physics and Applied Computer Science, Kraków, Poland
- ²⁹ National Center for Nuclear Research (NCBJ), Warsaw, Poland
- ³⁰ Horia Hulubei National Institute of Physics and Nuclear Engineering, Bucharest-Magurele, Romania
- ³¹ Petersburg Nuclear Physics Institute (PNPI), Gatchina, Russia
- ³² Institute of Theoretical and Experimental Physics (ITEP), Moscow, Russia
- ³³ Institute of Nuclear Physics, Moscow State University (SINP MSU), Moscow, Russia
- ³⁴ Institute for Nuclear Research of the Russian Academy of Sciences (INR RAN), Moscow, Russia
- ³⁵ Budker Institute of Nuclear Physics (SB RAS) and Novosibirsk State University, Novosibirsk, Russia
- ³⁶ Institute for High Energy Physics (IHEP), Protvino, Russia
- ³⁷ Universitat de Barcelona, Barcelona, Spain
- ³⁸ Universidad de Santiago de Compostela, Santiago de Compostela, Spain
- ³⁹ European Organization for Nuclear Research (CERN), Geneva, Switzerland
- ⁴⁰ Ecole Polytechnique Fédérale de Lausanne (EPFL), Lausanne, Switzerland
- ⁴¹ Physik-Institut, Universität Zürich, Zürich, Switzerland
- ⁴² Nikhef National Institute for Subatomic Physics, Amsterdam, The Netherlands
- ⁴³ Nikhef National Institute for Subatomic Physics and VU University Amsterdam, Amsterdam, The Netherlands
- ⁴⁴ NSC Kharkiv Institute of Physics and Technology (NSC KIPT), Kharkiv, Ukraine
- ⁴⁵ Institute for Nuclear Research of the National Academy of Sciences (KINR), Kyiv, Ukraine
- ⁴⁶ University of Birmingham, Birmingham, United Kingdom
- ⁴⁷ H.H. Wills Physics Laboratory, University of Bristol, Bristol, United Kingdom
- ⁴⁸ Cavendish Laboratory, University of Cambridge, Cambridge, United Kingdom
- ⁴⁹ Department of Physics, University of Warwick, Coventry, United Kingdom
- ⁵⁰ STFC Rutherford Appleton Laboratory, Didcot, United Kingdom
- ⁵¹ School of Physics and Astronomy, University of Edinburgh, Edinburgh, United Kingdom
- ⁵² School of Physics and Astronomy, University of Glasgow, Glasgow, United Kingdom
- ⁵³ Oliver Lodge Laboratory, University of Liverpool, Liverpool, United Kingdom
- ⁵⁴ Imperial College London, London, United Kingdom
- ⁵⁵ School of Physics and Astronomy, University of Manchester, Manchester, United Kingdom
- ⁵⁶ Department of Physics, University of Oxford, Oxford, United Kingdom
- ⁵⁷ Massachusetts Institute of Technology, Cambridge, MA, United States
- ⁵⁸ University of Cincinnati, Cincinnati, OH, United States
- ⁵⁹ University of Maryland, College Park, MD, United States
- ⁶⁰ Syracuse University, Syracuse, NY, United States
- ⁶¹ Pontifícia Universidade Católica do Rio de Janeiro (PUC-Rio), Rio de Janeiro, Brazil, associated to ²
- ⁶² University of Chinese Academy of Sciences, Beijing, China, associated to ³
- ⁶³ Institute of Particle Physics, Central China Normal University, Wuhan, Hubei, China, associated to ³
- ⁶⁴ Departamento de Física, Universidad Nacional de Colombia, Bogota, Colombia, associated to ⁸
- ⁶⁵ Institut für Physik, Universität Rostock, Rostock, Germany, associated to ¹²
- ⁶⁶ National Research Centre Kurchatov Institute, Moscow, Russia, associated to ³²
- ⁶⁷ Yandex School of Data Analysis, Moscow, Russia, associated to ³²
- ⁶⁸ Instituto de Física Corpuscular (IFIC), Universitat de Valencia-CSIC, Valencia, Spain, associated to ³⁷
- ⁶⁹ Van Swinderen Institute, University of Groningen, Groningen, The Netherlands, associated to ⁴²
- ^a Universidade Federal do Triângulo Mineiro (UFTM), Uberaba-MG, Brazil
- ^b Laboratoire Leprince-Ringuet, Palaiseau, France
- ^c P.N. Lebedev Physical Institute, Russian Academy of Science (LPI RAS), Moscow, Russia
- ^d Università di Bari, Bari, Italy
- ^e Università di Bologna, Bologna, Italy
- ^f Università di Cagliari, Cagliari, Italy
- ^g Università di Ferrara, Ferrara, Italy
- ^h Università di Genova, Genova, Italy
- ⁱ Università di Milano Bicocca, Milano, Italy
- ^j Università di Roma Tor Vergata, Roma, Italy
- ^k Università di Roma La Sapienza, Roma, Italy

^l *AGH - University of Science and Technology, Faculty of Computer Science, Electronics and Telecommunications, Kraków, Poland*

^m *LIFAEELS, La Salle, Universitat Ramon Llull, Barcelona, Spain*

ⁿ *Hanoi University of Science, Hanoi, Viet Nam*

^o *Università di Padova, Padova, Italy*

^p *Università di Pisa, Pisa, Italy*

^q *Università degli Studi di Milano, Milano, Italy*

^r *Università di Urbino, Urbino, Italy*

^s *Università della Basilicata, Potenza, Italy*

^t *Scuola Normale Superiore, Pisa, Italy*

^u *Università di Modena e Reggio Emilia, Modena, Italy*